Received May 2003
Revised June 2004
Accepted June 2004

A nonlinear numerical model for sloshing motion in tuned liquid dampers

M.R. Siddique and M.S. Hamed
Department of Mechanical Engineering, McMaster University, Hamilton, Ontario, Canada
A.A. El Damatty
Department of Civil and Environmental Engineering, University of Western Ontario, London, Ontario, Canada

Abstract

Purpose – This paper presents a new numerical model that, unlike most existing ones, can solve the whole liquid sloshing, nonlinear, moving boundary problem with free surface undergoing small to very large deformations without imposing any linearization assumptions.

Design/methodology/approach – The time-dependent, unknown, irregular physical domain is mapped onto a rectangular computational domain. The explicit form of the mapping function is unknown and is determined as part of the solution. Temporal discretization is based on one-step implicit method. Second-order, finite-difference approximations are used for spatial discretizations.

Findings – The performance of the algorithm has been verified through convergence tests. Comparison between numerical and experimental results has indicated that the algorithm can accurately predict the sloshing motion of the liquid undergoing large interfacial deformations.

Originality/value – The ability to model liquid sloshing motion under conditions leading to large interfacial deformations utilizing the model presented in this paper improves our ability to understand the problem of sloshing motion in tuned liquid dampers (TLDs), which would eventually help in constructing more effective TLDs.

Keywords Finite difference methods, Boundary-elements methods, Liquids, Deformation

Paper type Research paper

Nomenclature

A	= amplitude of the external dynamic excitation, m	L	= length of the tank, m
b	= width of the tank, m	P	= pressure, Pa
Ca	= capillary number	q	= any variable
f_e	= frequency of the applied external excitation, Hz	Re	= Reynolds number
f_0	= natural frequency of the structure, Hz	t	= time, s
f_w	= fundamental sloshing frequency of the contained liquid in tank, Hz	u,v	= velocity components in the horizontal and vertical directions, respectively, m/s
Fr	= Froude number	u_c	= characteristic velocity, m/s
g	= gravitational acceleration, m/s^2	V	= volume of the liquid, m^3
h	= height of the free surface, m	x,y	= Cartesian coordinates
H	= height of the initial flat free surface, m	X	= time dependent displacement, m
		θ	= contact angle

International Journal for Numerical Methods in Heat & Fluid Flow
Vol. 15 No. 3, 2005
pp. 306-324

0961-5539
DOI 10.1108/09615530510583900

Greek letters

β = error level
ε = aspect ratio
ξ, η = mapped coordinates
ψ = stream function
ρ = density, kg/m^3
μ = dynamic viscosity, N s/m^2
σ = surface tension, N/m
Ω = computational domain
ω = vorticity

Subscripts

x, y, t, ξ, η = partial derivatives with respect to the variable x, y, t, ξ, η

1. Introduction

A tuned liquid damper (TLD) is a passive damping device proven to be effective in controlling the vibration of structures and systems in many engineering applications. Unlike active or semi-active dampers, passive dampers do not require any external supply of power to operate (Soong and Dargush, 1997). The main function of a passive damping device is to absorb a portion of the input energy associated with external dynamic excitations acting on a structure, thus minimizing or avoiding structural damages. Other types of passive dampers include metallic, tuned mass, and viscoelastic dampers.

A TLD consists of one or multiple rigid tanks, partially filled with a liquid, usually water. The tanks are rigidly attached to the structure. The vibration of the structure under an external dynamic load causes sloshing motion of the contained liquid. By tuning the natural frequency of this sloshing motion to the natural frequency of the structure, the liquid motion imparts inertia forces approximately anti-phase to the dynamic forces exciting the structure, thereby reducing structural motion. As such, the attachment of TLDs modifies the frequency response of the structure in a way similar to increasing its effective damping.

The use of TLDs is increasing due to their many advantages over other conventional damping devices. TLDs can be used for both small- (wind) and large-amplitude (earthquake) vibrations. They are easy to install to existing structure, and need low maintenance and operating cost. TLDs were used in marine vessels to stabilize against rocking and rolling motions (Watanabe, 1969; Matsuuara *et al.*, 1986), offshore platforms (Vandiver and Mitone, 1978; Lee and Reddy, 1982), and in tall structures (Kareem and Sun, 1987; Tamura *et al.*, 1988; Noji *et al.*, 1988; Fujii *et al.*, 1990; Wakahara *et al.*, 1992; Wakahara, 1993). Although the construction of a TLD is simple, the liquid sloshing motion inside the tank has a highly nonlinear and complex behavior. Surface slopes can approach infinity and the liquid may encounter the top cover in enclosed tanks. The amplitude of the sloshing motion depends on the nature, amplitude and frequency of the applied external excitation, the geometry of the tank and the depth and properties of the contained liquid (Koh *et al.*, 1994; Celebi and Akyildiz, 2002). In order to design an efficient and effective TLD, the sloshing behavior of the liquid has to be well understood.

The sloshing behavior of liquid in tanks under dynamic loads was studied extensively through experimental investigations (Cooper, 1960; Abramson, 1966; Chester, 1968; Miles, 1976; Clough *et al.*, 1978). Numerical modeling of the sloshing behavior of liquids was investigated mostly by simplified linear theories that are applicable only to small interfacial deformations. Potential flow theory, which considers inviscid, irrotational flows, was widely used by many researchers (Nakayama and Washizu, 1981; Nakayama, 1983; Ohyama and Fujii, 1989; Tosaka and Sugino, 1991; Chen *et al.*, 1996; Warnitchai and Pinkaew, 1998; Dutta and Laha, 2000). Shallow water

wave theory was also applied by others (Shimizu and Hayama, 1987; Reed *et al.*, 1998), where the wave height or the amplitude of the interfacial deformation is assumed to be small compared to the mean depth of the liquid layer, and the horizontal velocity is uniform throughout the depth. A number of studies (Sun *et al.*, 1989; Fujino *et al.*, 1992; Sun and Fujino, 1994; Sun *et al.*, 1995) combined the shallow water theory with the boundary layer theory, where the liquid viscosity is considered only in the boundary layer region.

An improvement over predictions based on potential flow theory was provided by Zang *et al.*(2000) using a linearized form of Navier-Stokes equations by neglecting the convective acceleration terms. They indicated that liquid viscosity has an important effect on sloshing motion near rigid walls, especially with excitation frequency near resonance.

The linear theory is applicable only when the amplitude of interfacial deformations are expected to be small. This is valid in cases of small external amplitudes or at frequency of excitation away from the natural frequency of the TLD. Consequently, when the excitation of the oscillation is near the natural frequency of the TLD, or excitation amplitude is high, the linear model becomes inadequate (Lepelletier and Raichlen, 1988).

Ramaswamy *et al.* (1986) have solved the full nonlinear Navier-Stokes equations using the Lagrangian finite element and the velocity correction method for two-dimensional liquid sloshing problems. Only small amplitude oscillation was considered in the study, where the behavior of the liquid sloshing is linear.

A TLD is usually designed to operate at or near the resonant frequency of the structure in order to maximize the absorbed and dissipated energy. To predict accurately sloshing motion inside a TLD, a numerical model should: first, consider all physical effects (inertia and viscosity), and secondly, be able to solve such moving boundary problem while allowing large interfacial deformations.

Algorithms for moving boundary problems were reviewed by Floryan and Rasmussen (1989). Moving free surface can be described either in terms of fixed grids, adaptive grids, or by applying analytical mapping techniques. In the third approach, analytical mapping transfers the problem from an irregular physical domain onto a rectangular computational domain. The mapping function is unknown and has to be determined as part of the solution procedure. Since this approach is computationally more efficient and accurate, it has been selected as the base of the present work.

The study starts by describing the mathematical formulation of the sloshing problem in Section 2. The structure of the applied numerical algorithm is outlined in Section 3. An overview of the experimental set up used to validate this model is given in Section 4. A convergence study as well as comparison with experimental results are presented in Section 5 that is followed by the conclusions summarized in Section 6.

2. Mathematical formulation

Consider a rigid rectangular tank of length L, filled with water to a stationary depth H, as shown in Figure 1. The coordinate system is attached to the tank with the origin located at the center of the bottom. The tank is subjected to a general external harmonic excitation in the horizontal (x) direction, defined by time dependent displacement $X(t)$. Thereby neglecting the end effects, the motion of the liquid inside the tank can be assumed to be two-dimensional in the x-y directions.

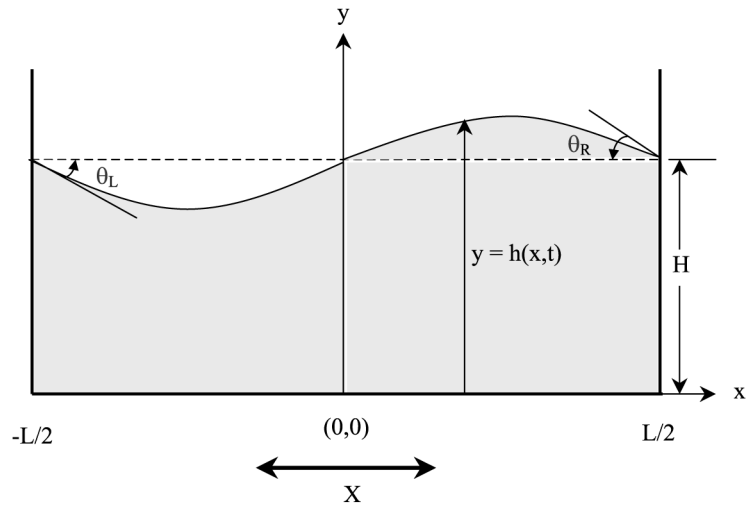

Figure 1.
Physical domain in x, y coordinates

The liquid inside the tank is assumed to be Newtonian, viscous, and incompressible. Thus, the transient two-dimensional motion of the liquid inside the tank is governed by the continuity and the x- and y- momentum equations. The governing equations as well as the boundary conditions are non-dimensionalized by introducing the following dimensionless variables:

$$x^* = \frac{x}{L}, \quad y^* = \frac{y}{H}, \quad u^* = \frac{u}{u_c}, \quad v^* = \frac{v}{\varepsilon u_c}, \quad p^* = \frac{p}{\mu u_c L/H^2}, \quad t^* = \frac{t}{H/u_c}, \quad X^* = \frac{X}{H} \quad h^* = \frac{h}{H}. \tag{1}$$

where the superscript $*$ denotes dimensionless variables, u and v are the x and y components of the velocity vector, respectively, p the pressure, t stands for time, μ the dynamic viscosity of the liquid, and the aspect ratio of the liquid layer in the tank is defined by the dimensionless parameter, $\varepsilon = H/L$. The characteristic velocity, u_c, is defined by $u_c = \sqrt{gH}$, where g is the gravitational acceleration.

The governing equations in dimensionless form (with the superscript $*$ dropped) are:

$$u_x + v_y = 0, \tag{2}$$

$$\mathrm{Re}[u_t + \varepsilon(uu_x + vu_y)] = -p_x + \varepsilon^2 u_{xx} + u_{yy} - \mathrm{Re}\, X_{\mathrm{tt}}, \tag{3a}$$

$$\varepsilon^2\, \mathrm{Re}[v_t + \varepsilon(uv_x + vv_y)] = -p_y + \varepsilon^2(\varepsilon^2 v_{xx} + v_{yy}) - \varepsilon^2 \frac{\mathrm{Re}}{\mathrm{Fr}^2} \tag{3b}$$

where the subscripts x, y, and t denote partial derivatives with respect to x, y, and t, respectively, and X_{tt} is the acceleration due to time dependent known external excitation. In the above equations, Re and Fr stand for the Reynolds number, and the Froude number, respectively, defined as follows:

$$\mathrm{Re} = \frac{\rho u_c H}{\mu}, \quad Fr = \frac{u_c}{\sqrt{gL}}. \tag{4}$$

where ρ is the density of the liquid. The above governing equations (2) and (3) are subject to the following boundary conditions:

$$\text{at } x = \pm 1/2, \quad u = v = 0 \tag{5}$$

$$\text{at } y = 0, \quad u = v = 0. \tag{6}$$

The interface is defined by the function $h(x)$, which will be determined as part of the solution procedure. Boundary conditions at the interface are:

$$\text{at } y = h(x,t), \quad h_t + \varepsilon(uh_x - v) = 0, \tag{7a}$$

$$-p + \frac{2\varepsilon^2[v_y - h_x u_y + \varepsilon^2 h_x(u_x h_x - v_x)]}{\left(1 + \varepsilon^2 h_x^2\right)} = \frac{\varepsilon^3 h_{xx}}{\mathrm{Ca}\left(1 + \varepsilon^2 h_x^2\right)^{3/2}}, \tag{7b}$$

$$2\varepsilon^2 h_x(v_y - u_x) + \left(1 - \varepsilon^2 h_x^2\right)(\varepsilon^2 v_x + u_y) = 0. \tag{7c}$$

where Ca is the capillary number defined by $\mathrm{Ca} = \mu u_c/\sigma$ and σ is the surface tension.

Equations (5) and (6) are the no-penetration and no-slip conditions at the rigid walls of the tank. The kinematic condition at the free surface is given by equation (7(a)). Equation (7(b) and (c)) are the dynamic condition at the free surface representing the balance of the normal and tangential stresses at the interface, respectively. The deforming free surface must also satisfy the following mass conservation constraint:

$$\int_{-1/2}^{1/2} h(x,t)\mathrm{d}x = \forall^*. \tag{8}$$

where the dimensionless volume $\forall^* = V/HL$ with unit dimension perpendicular to the xy-plane. The problem is closed by specifying the contact conditions between the free surface and the sidewalls:

$$h(-1/2) = \frac{\tan\theta_L}{\varepsilon}, \quad h(1/2) = \frac{-\tan\theta_R}{\varepsilon} \tag{9}$$

where the prescribed contact angle θ depends on the tank material and the type of liquid.

Equations (2)-(9) constitute a moving boundary problem, where the location of the free surface is time dependent and has to be determined as part of the solution.

2.1 Coordinate transformation

The liquid layer inside the tank has a moving free surface which makes it an irregular, time-dependent solution domain (as defined by $h(x,t)$). The solution domain Ω (x, y) is mapped onto a rectangular computational domain Ω^* (ξ,η) as shown in Figure 2 permitting use of standard finite-difference discretization techniques for spatial

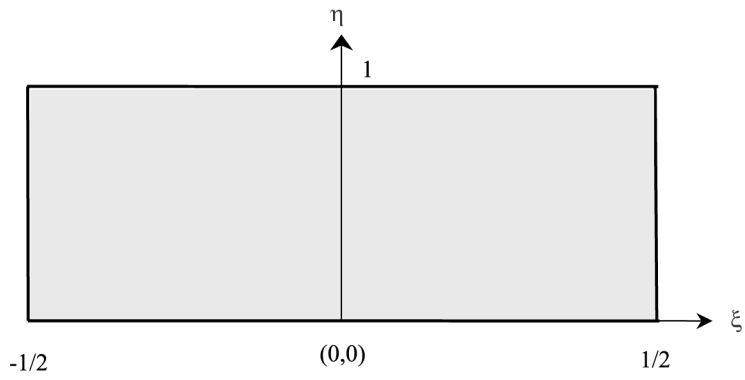

Figure 2.
Computational domain in ξ, η coordinates

derivatives. The explicit form of the mapping function $h(x, t)$ is not known and has to be determined as part of the numerical procedure. The transformation used in this case is:

$$\xi = x, \quad \eta = \frac{y}{h(x,t)}. \tag{10}$$

2.2 Stream function-vorticity formulation

The use of the stream function-vorticity formulation permits a simple enforcement of the incompressibility condition (equation (2)), which is crucial in the case of a free boundary problem. The stream function, ψ, and vorticity, ω, in dimensionless form are defined as follows:

$$u = \psi_y, \quad v = -\psi_x, \quad \omega = -\varepsilon^2\psi_{xx} - \psi_{yy}. \tag{11}$$

The governing equations (2) and (3) in the transformed coordinate system reduce to:

$$\nabla^2\psi + \omega = 0, \tag{12}$$

$$\omega_t - \frac{\eta h_t \omega_\eta}{h} + \frac{\varepsilon(\psi_\eta\omega_\xi - \psi_\xi\omega_\eta)}{h} = \frac{\nabla^2\omega}{\mathrm{Re}}, \tag{13}$$

where

$$\nabla^2 = \varepsilon^2\frac{\partial^2}{\partial\xi^2} - \frac{2\varepsilon^2\eta h_\xi}{h}\,\frac{\partial^2}{\partial\xi\,\partial\eta} + \frac{\left(1+\varepsilon^2\eta^2h_\xi^2\right)}{h^2}\,\frac{\partial^2}{\partial\eta^2} + \frac{\eta\varepsilon^2\left(2h_\xi^2 - hh_{\xi\xi}\right)}{h^2}\,\frac{\partial}{\partial\eta}. \tag{14}$$

The boundary conditions (equations (5)-(7)) take the form:

$$\text{at } \xi = \pm 1/2, \quad \psi = \psi_\xi = 0, \tag{15}$$

$$\text{at } \eta = 0, \quad \psi = \psi_\eta = 0, \tag{16}$$

$$\text{at } \eta = 1, \quad h_t + \psi_\xi = 0, \tag{17a}$$

$$-p + \frac{2\left|\varepsilon^4 h_\xi \psi_{\xi\xi} - \left(1 + h_\xi^2\right)\varepsilon^2 \psi_{\xi\eta} h^{-1} + \varepsilon^2 h_\xi \left(1 + \varepsilon^2 h_\xi^2 - \varepsilon^2 h h_{\xi\xi}\right)\psi_\eta\right|}{\left(1 + \varepsilon^2 h_\xi^2\right)}$$

$$= \frac{\varepsilon^3 h_{\xi\xi}}{\mathrm{Ca}\left(1 + \varepsilon^2 h_\xi^2\right)^{3/2}}, \tag{17b}$$

$$\begin{aligned} &- \varepsilon^2\left(1 - \varepsilon^2 h_\xi^2\right)\psi_{\xi\xi} + \frac{\left(1 + \varepsilon^2 h_\xi^2\right)^2}{h^2}\psi_{\eta\eta} - \frac{2\varepsilon^2 h_\xi \left(1 + \varepsilon^2 h_\xi^2\right)}{h}\psi_{\xi\eta} \\ &+ \frac{\left[\varepsilon^2\left(1 - \varepsilon^2 h_\xi^2\right)h h_{\xi\xi} + 2\varepsilon^2 h_\xi^2\left(1 + \varepsilon^2 h_\xi^2\right)\right]}{h^2}\psi_\eta = 0. \end{aligned} \tag{17c}$$

The boundary conditions for ω at the solid walls and interface are obtained from equation (12) and given below:

$$\text{at } \xi = \pm 1/2, \quad \omega = -\varepsilon^2 \psi_{\xi\xi} \tag{18a}$$

$$\text{at } h = 0, \quad \omega = -\frac{1}{h^2}\psi_{\eta\eta} \tag{18b}$$

$$\text{at } \eta = 1, \quad \omega = -2\left(1 + h_\xi^2\right)^{-1}\psi_{\xi\xi} + h^{-1}\left(1 + h_\xi^2\right)^{-1}(2h_{\xi\xi}\psi_\eta) \tag{18c}$$

The normal stress condition (equation (17(b))) involves the value of pressure at the interface, which has to be determined on the basis of the known solution of the flow field. Equation (3(a) and (b)) are solved for components of the pressure gradient, transformed into the (ξ,η) plane using equation (10), expressed in a form suitable for the interface ($\eta = 1$), and integrated with respect to ξ using the trapezoidal rule based on the same grid as used in the determination of the flow field. More details about the calculation of the pressure at the interface can be found in Hamed and Floryan (1998).

2.3 Finite-difference discretization

Spatial derivatives are discretized over the rectangular computational domain using standard second-order finite-difference formulas. Thus, the algorithm is second-order accurate in space. Hamed and Floryan (1998) have studied one- and two-step implicit, Crank-Nicolson, trapezoidal temporal discretization schemes for a nonlinear moving boundary cavity problem and found that the one-step method is self-starting and numerically stable. Therefore, this discretization method has been used for temporal derivatives in the present study.

3. The algorithm

The solution procedure is initiated by assuming that all variables are known at time $t = n\Delta t$ and their values at $t = (n + 1)\Delta t$ are sought. Here Δt is the time step, and n is

an index for the time step with $n = 0$ at $t = 0$. Assuming a flat interface at $t = 0$, the field equations (12) and (13) are solved iteratively keeping the location of the free surface and the value of the stream function at the free surface unchanged and enforcing all boundary conditions except the normal stress (equation (17(b))) and the kinematic conditions (equation (17(a))). This problem will be referred as the "inner problem" or the "inner solution". After solving the field equations by inner iterations, the normal stress condition is used subsequently to determine the new location of the free surface then the kinematic condition is employed to evaluate the new value of the stream function at the free surface. This part of the solution will be referred as the "outer problem" or the "outer solution". The complete solution procedure involves iterations between the inner and the outer problems until the convergence criteria, $|q_{i+1} - q_i| < \beta_1$ and $|\mathrm{Res}_i| < \beta_1$ with $\beta_1 = 10^{-7}$ are satisfied at all grid points. The variable q stands for any of the flow quantities (ψ, ω) and Res denotes residuum of any of the discretized field equations, and subscript i denotes the iteration number. The flow chart illustrating this iterative procedure is shown in Figure 3. More details of the numerical algorithm and the iterative solution procedure can be found in Hamed and Floryan (1998).

4. Experimental study

An experimental investigation has been carried out by Tait *et al.* (2001) at the Boundary-Layer Wind Tunnel Laboratory of the University of Western Ontario using a prototype of an actual TLD tank. The TLD shown in Figure 4 represents a 1:10 model of one of the multiple tanks designed to be attached to a real building having a fundamental frequency of approximately 0.172 Hz. The dimensions L, b, and H represent the tank length in the direction of external excitation, the tank width (perpendicular to excitation) and the still water depth, respectively. The fundamental sloshing frequency, f_w, for the water inside this tank can be calculated according to the linear wave theory using the following equation (Lamb, 1932):

$$f_w = \frac{1}{2\pi}\sqrt{\frac{\pi g}{L}\tanh\left(\frac{\pi H}{L}\right)} \tag{19}$$

Substituting the values of L and H as given in Figure 4 into the above equation gives $f_w \approx 0.545$ Hz. Using dimensional analysis, the fundamental liquid sloshing frequency of the prototype tank is estimated to be equal to $f_w/\sqrt{10} = 0.172$ Hz. This means that the sloshing frequency of the prototype tank was tuned to the fundamental frequency of the building. The tuning frequency Ω, is an important parameter which strongly influences the performance of a TLD, and is given by $\Omega = f_w/f_0$, where f_0 is the natural frequency of the structure.

A schematic diagram of the experimental set up is shown in Figure 5. The set up included a rigid support frame attached to a shake table. The TLD was attached to the top part of the frame using four cables that provided only vertical support for the tank. The lateral support of the tank was provided by two load cells that connected the bottom of the tank to the rigid intermediate member of the frame. The data recorded included the shaking table displacement, the base shear forces developed by both the TLD and ballast masses and temporal free surface at six locations simultaneously along the tank using capacitance type wave probes. Details of the experimental study can be found in Tait *et al.* (2001).

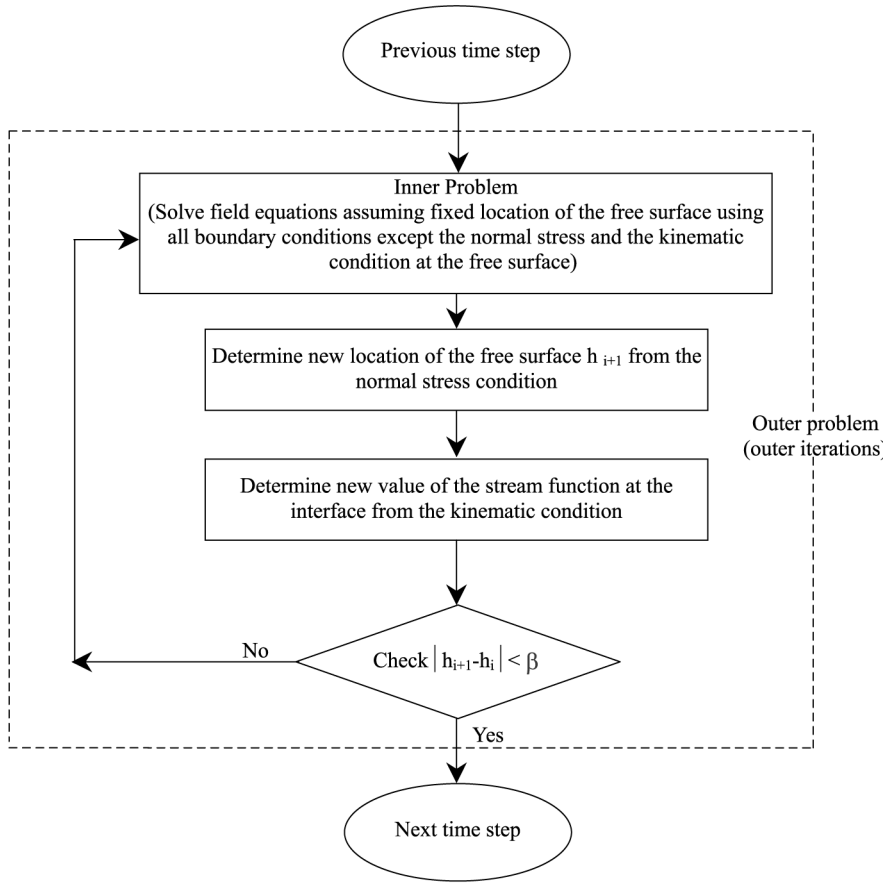

Figure 3.
Flow chart for the solution algorithm

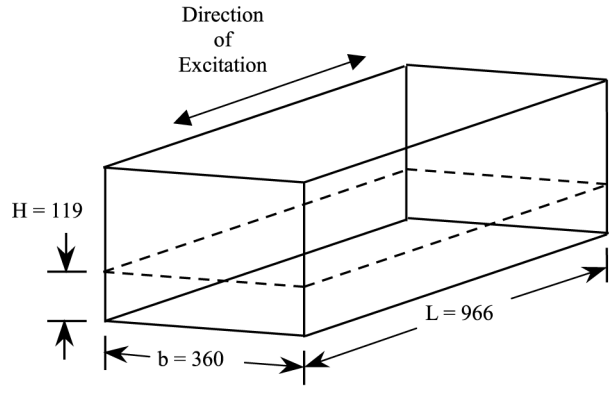

Figure 4.
Tuned liquid damper used in the experimental study (dimensions are in mm)

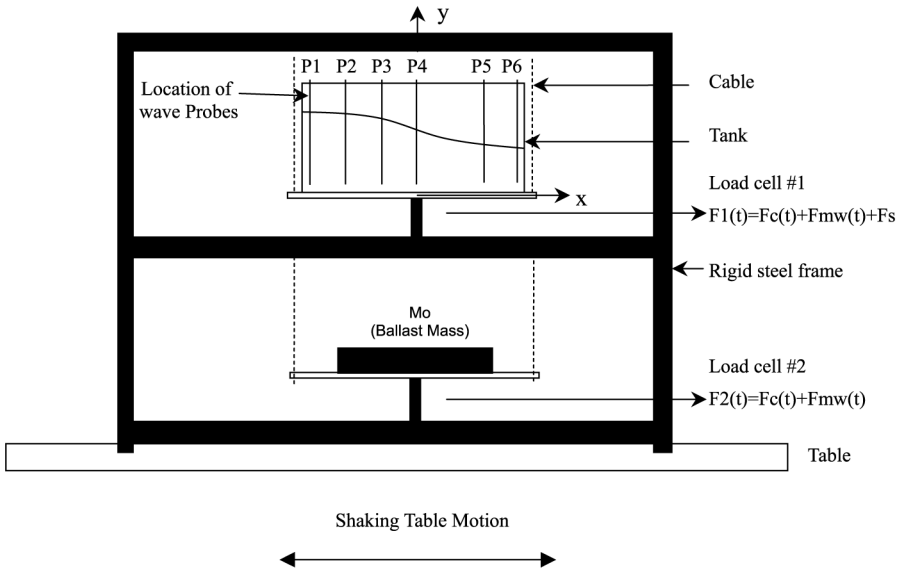

Figure 5.
Shaking table test set up (location of wave probes from the left wall of the tank, $P1 = 0.048$ m, $P2 = 0.193$ m, $P3 = 0.338$ m, $P4 = 0.483$ m, $P5 = 0.773$ m, $P6 = 0.917$ m)

The frame assembly was subjected to sinusoidal excitation with excitation amplitude of 2.5 mm. The tests were conducted at the excitation frequency of $f_e = 0.545$ Hz. The water was quiescent at the start of all tests conducted, and the data were recorded after the liquid sloshing motion reached a steady-state condition. Steady-state condition was reached when the interface deformations recorded at the six locations shown in Figure 5 were not changing with time.

5. Algorithm performance

In this section, the numerical model is first assessed for grid convergence. Then the numerical algorithm is validated by comparing the numerical and the experimental results. Finally, the effects of the amplitude of the external excitation on the sloshing amplitude and the base shear force are investigated.

The dimensions of the tank for numerical simulation match exactly the one used in the experimental study shown in Figure 4. The tank is assumed to be subjected to a horizontal sinusoidal displacement defined by $X = A\sin(2\pi f_e t)$, where A is the amplitude, f_e is the frequency of the external excitation in hertz, and t is the time in second. All numerical results are computed at excitation frequency matching the natural frequency of the liquid in the tank, i.e. at $f_e = 0.545$ Hz. Since the liquid in the tank is water, the contact angle at both left and right side walls, θ, is assumed to be zero.

5.1 Grid convergence

The computational time and error in the solution are functions of the grid size The effect of the grid size on the solution is investigated to determine the optimum size to get solution with satisfactory accuracy within reasonable computational time. Five different sets of grids are examined, 11×11, 15×15, 21×21, 26×26, and 31×31.

The grid convergence of the algorithm is assessed based on the change in both the deformation of the free surface and the amount of the base shear force. During this grid convergence study the size of the time step was kept constant at 0.01 s, which is 1/183 of one period of the external sinusoidal excitation.

The height of the free surface at the left wall and the base shear force after reaching steady-state using the five different grid sizes, are shown in Figure 6. The horizontal axis in the figure represents the time relative to the instant at which the motion reached steady-state, which happened after about 60 s from the initial application of the

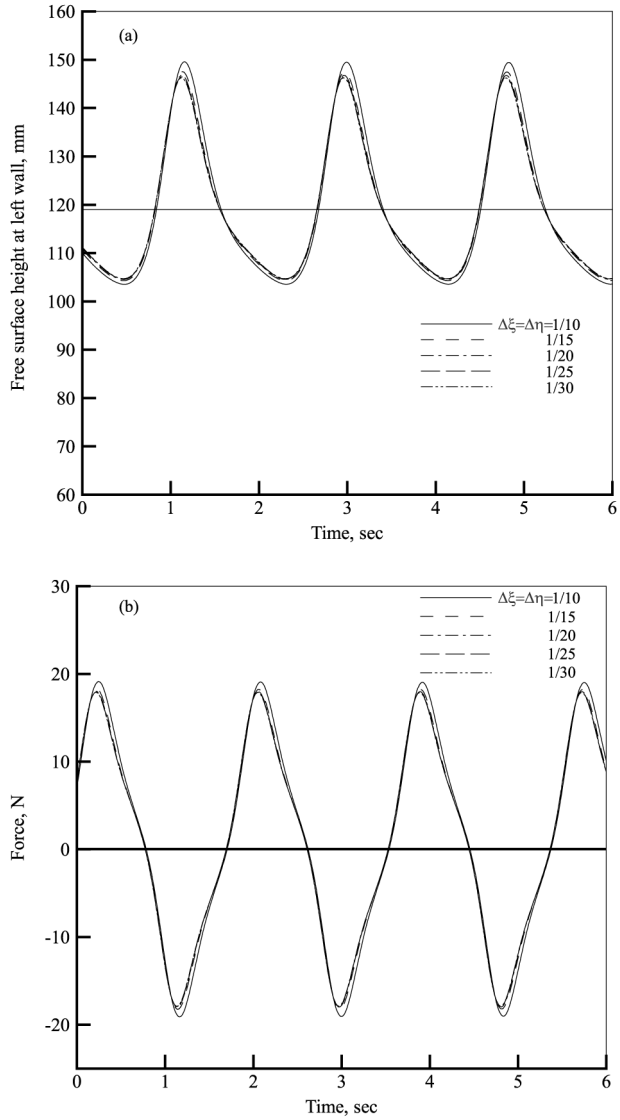

Figure 6.
Effect of gird size on the steady-state: (a) free surface deformation at the left wall ($x = -L/2$); and (b) base shear force; f_e= 0.545 Hz, $A = 2.5$ mm, $\Delta t = 0.01$ s

external excitation. The figure shows that the solution is converging as the grid size is being refined. In order to determine the optimum grid size, the solution with grid size 1/30 is considered as the reference solution. The maximum relative changes with respect to the reference solution in both the height of the free surface at the left wall and the base shear force are given in Table I. The table shows that the convergence rate is very fast. The relative changes using the 1/10 coarse grid are about 2 and 7 percent in both the height of the free surface and the base shear force, respectively. However, the corresponding relative changes were decreased to less than 1 percent with a grid size of 1/20.

The effect of grid size on the shape of the whole free surface of the sloshing fluid along the tank length is shown in Figure 7 at two different times, after reaching the steady-state. The two plots indicate that the coarse grid 1/10 produces a significantly different solution compared to the reference grid, 1/30. This difference is strongly reduced using the next grid, 1/15, indicating a fast convergence rate. Because the relative change in the free surface between grid sizes 1/30 and 1/20 was less than 0.2 percent, it was concluded that grid size 1/20 is sufficient to capture a satisfactory converged solution.

The size of the time step also influences the accuracy of the numerical solution. The time step has to be small enough to accommodate the effect of sufficient number of high vibration modes that contribute to the fluid motion. The effect of time step on the height of the free surface at the left wall is shown in Figure 8. The figure shows the steady-state variation in the height of the free surface for three different time steps. The smallest time step, 0.005 s, represents the most accurate solution. When used as a reference, the maximum difference in wave height compared to the other two time steps, 0.02 and 0.01 s, were about 10 and 3.7 percent, respectively. Owing to the convergent nature of the solution, it was expected that if the time step was further reduced by a factor of 2 (i.e. using 0.0025 s time step), the difference in the maximum wave height compared to that obtained with the 0.005 s time step would be less than 3.7 percent, which was considered an acceptable level of accuracy, and therefore, the time step of 0.005 s was used in this study.

5.2 Algorithm validation

The developed numerical model has been validated by comparing the numerical results to the corresponding experimental values The numerical results presented here were obtained using a 21×21 grid, and a time step of 0.005 s. The amplitude of the sinusoidal excitation is 2.5 mm in both experimental and numerical studies.

Grid size, $\Delta\xi = \Delta\eta$	Relative change in free surface at left wall (percent)	Relative change in base shear force (percent)
1/10	2.3	6.9
1/15	0.9	2.0
1/20	0.4	0.6
1/25	0.1	0.15
1/30	0	0

Table I. Influence of the grid size on the solution, $f_e = 0.545$ Hz, $A = 2.5$ mm, $\Delta t = 0.01$ s

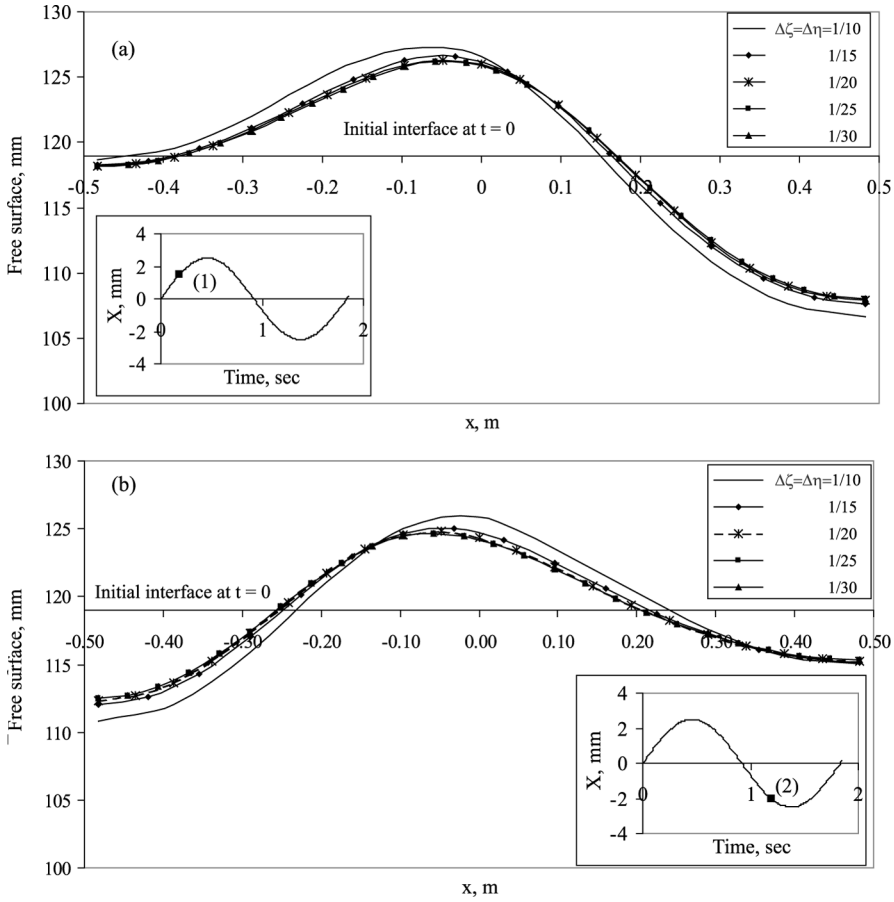

Figure 7.
Effect of gird size on the free surface elevation along the tank length at time: (a) 60.75 s (point 1, external displacement, $X = +1.6$ mm), maximum deformation = 11 percent of H; and (b) 61.75 s (point 2, external displacement, $X = -2.05$ mm), maximum deformation = 7 percent of H; f_e=0.545 Hz, $A = 2.5$ mm, $\Delta t = 0.01$ s

The numerical and experimental results for the free surface deformation at three locations along the tank length as well as for base shear force are shown in Figure 9(a) and (d). The presence of the higher or super harmonics was observed in the experimental results. The behavior of the free surface is almost identical in both experimental and numerical results for all three locations shown, except the presence of the higher harmonics is not very clear in the numerical results. It is expected that the higher harmonics would not affect the base shear force. The maximum and minimum interface deformation is almost equal at all three locations. The maximum change in the free surface at the left wall of the numerical solution is less than 2 percent compared to the experimental value. There is a very good agreement between the numerically obtained and experimentally measured base shear force values. The maximum difference in the numerically predicted base shear force compared to the experimentally measured value is about 5 percent. The very good agreement between the experimental and the numerical results in both free surface wave and base shear force clearly indicates the validity of the developed numerical model.

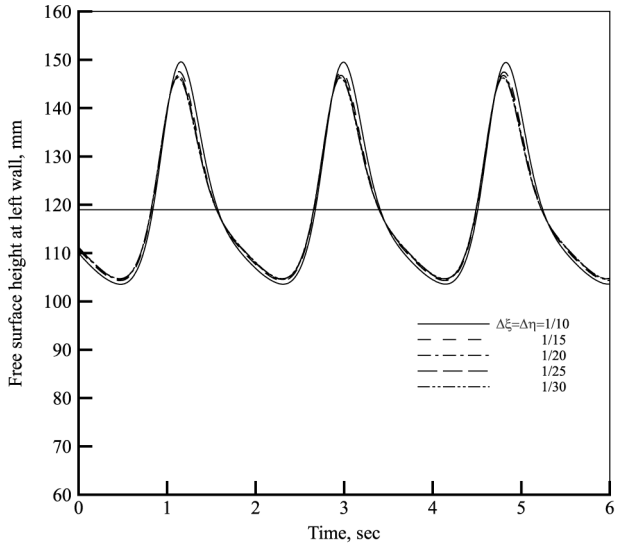

Figure 8.
Effect of time step size on free surface at the left wall ($x = -L/2$), f_e=0.545 Hz, A = 2.5 mm, $\Delta\xi = \Delta\eta = 1/20$

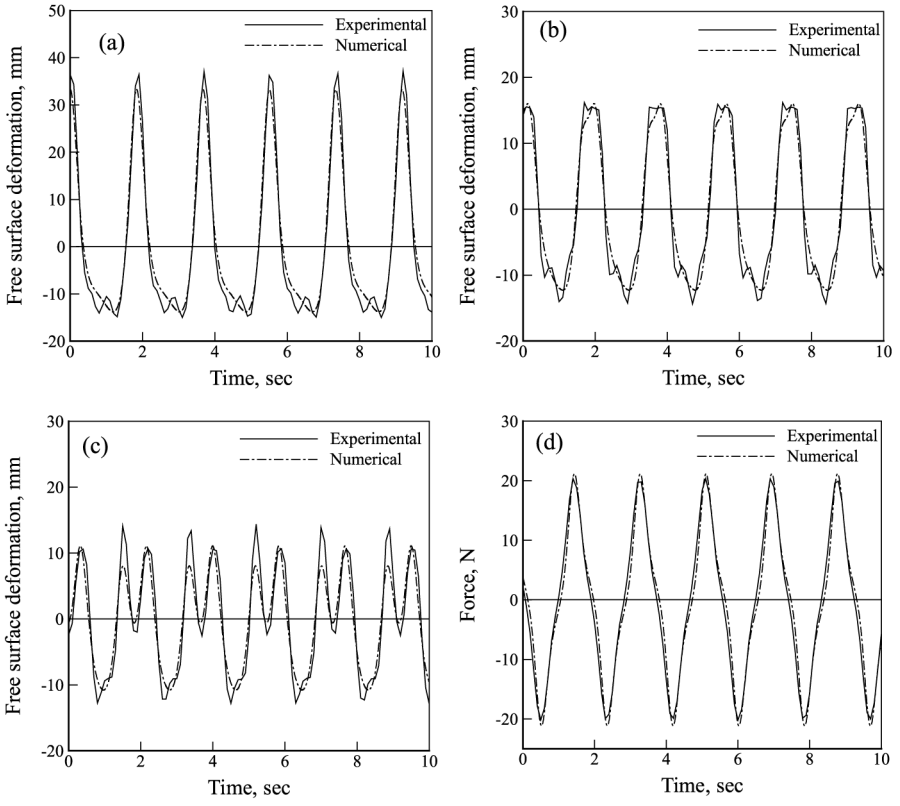

Figure 9.
Steady-state free surface deformation at: (a) 0.0483 m; (b) 0.193 m; (c) 0.338 m from left wall; and (d) base shear force; f_e=0.545 Hz, Δt = 0.005 s, $\Delta\xi = \Delta\eta = 1/20$

5.3 Numerical results

The entire time histories, including the transient period of the deformation of the free surface motion at the left wall as well as the base shear force are shown in Figure 10 for excitation amplitude of 2.5 mm and frequency of 0.545 Hz. The figure indicates that the steady-state condition is reached approximately after 60 s. It is also shown that the maximum values of the transient response (both wave height and base shear force) are slightly higher than the steady-state values. The maximum transient and steady-state deformations are around 26 and 23 percent of the initial depth of the water layer, respectively. The maximum transient base shear force is around 8 percent higher than the corresponding steady-state value. A three-dimensional plot showing the time and space variation of the steady-state free surface wave is shown in Figure 11. It can be seen from both Figures 10(a) and 11 that the free surface deformation is asymmetric about the initial still water level. The free surface elevation in the upward direction is larger than that in the downward direction. Such nonlinearity of liquid motion is also observed experimentally (Figure 9(a) and (b)). It is interesting to notice that although the maximum upward and downward values of the surface wave are not equal, the maximum positive and negative values for base shear force remains identical. This coincides with the experimental findings as shown in Figure 9(d).

The amplitude of the liquid sloshing strongly depends on the nature, amplitude and frequency of the tank motion. Figure 12 shows variation of the maximum deformation of the free surface and the maximum base shear force with the amplitude of external excitation for both the transient and the steady-state domains. The plots indicate that the difference between the transient-maximum and

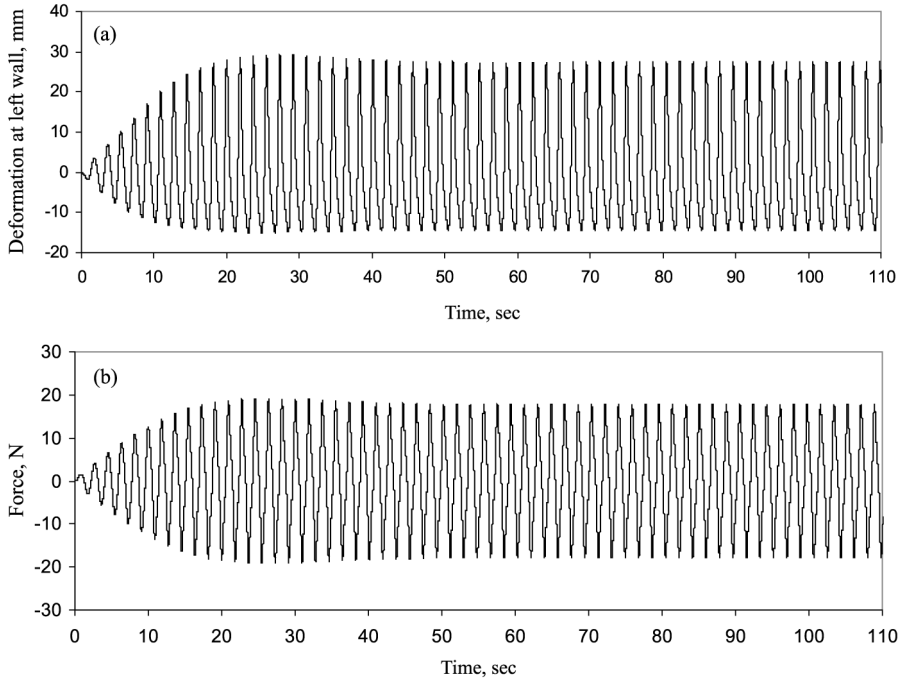

Figure 10.
Time histories of the: (a) free surface deformation at the left wall ($x = -L/2$); and (b) base shear force; f_e=0.545 Hz, $A = 2.5$ mm, $\Delta t = 0.01$ s, $\Delta\xi = \Delta\eta = 1/20$

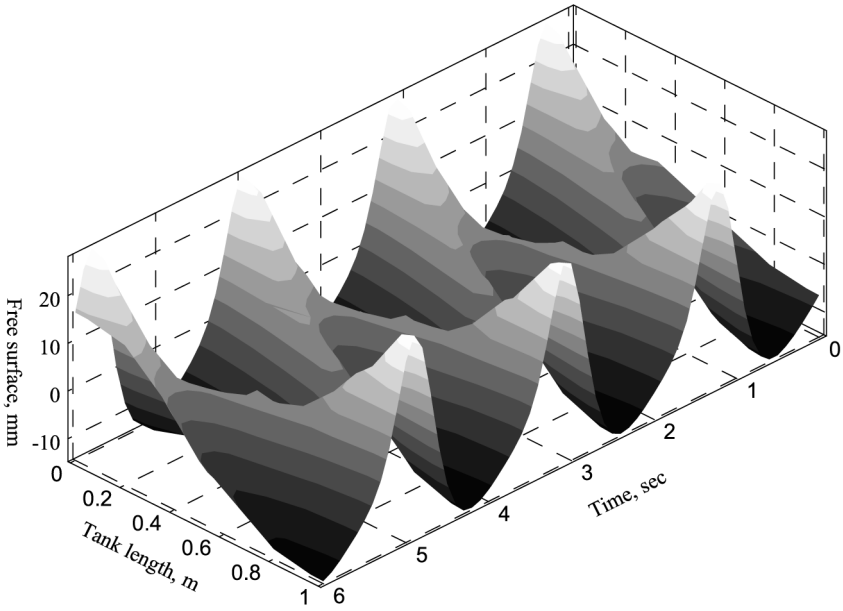

Figure 11.
Steady-state time histories of the free surface deformation along the tank length, f_e=0.545 Hz, $A = 2.5$ mm, $\Delta t = 0.01$ s, $\Delta\xi = \Delta\eta = 1/20$

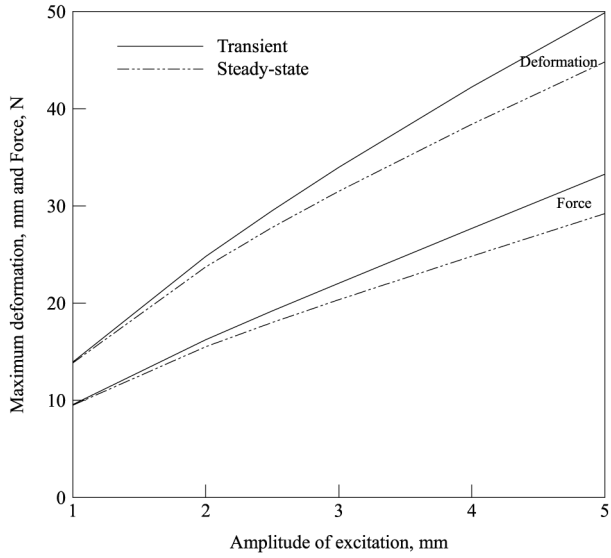

Figure 12.
Effect of amplitude on the maximum free surface deformation at the left wall ($x = -L/2$) and base shear force; f_e=0.545 Hz, $\Delta t = 0.01$ s, $\Delta\xi = \Delta\eta = 1/20$

steady-state-maximum free surface response increases as the amplitude of the external excitation increases. The maximum transient deformations with external excitation amplitudes of 1 and 5 mm are around 12 and 42 percent of the initial depth of the water level, respectively. The plots also indicate that a nonlinear behavior with excitation amplitude is more obvious for the liquid sloshing compared to the base

shear force. The nonlinear behavior of the liquid sloshing is further shown in Figure 13, where the steady-state deformations of the free surface at the left wall of the tank are shown for the three levels of excitation amplitudes. The behavior of the liquid sloshing at smaller amplitude (1.25 mm) is linear which is recognized by the fact that the free surface deformation is symmetric about the initial still water level. As the amplitude of the external excitation increases (2.5 and 5 mm), the nonlinear behavior emerges, where the free surface deformation in the upward direction is larger than that in the downward direction.

6. Conclusions

A numerical model was developed to simulate the transient, nonlinear, two-dimensional sloshing motion inside a tank of a tuned liquid damper undergoing arbitrary interface deformation. The model is based on the vorticity-stream function formulation. The unknown time-dependent solution domain is mapped onto a fixed rectangular computational domain with the explicit form of the time-dependent mapping function to be determined as a part of the solution procedure. To show the effectiveness of the developed numerical model for large interface deformation, simulations were performed at the natural frequency of the contained liquid that was previously tested experimentally under harmonic excitations. The numerical results in terms of free surface deformation and base shear force are compared with the corresponding experimental values. Excellent agreement was found between the numerical and experimental results at such large interface deformation. The amplitude of the external excitation is found to have a strong effect on the sloshing behavior of the liquid in the tank. The liquid sloshing is found to be linear at smaller amplitudes and gradually emerges to a nonlinear type of behavior as the amplitude level increases. Less nonlinear variation with excitation amplitude is observed for the base shear force.

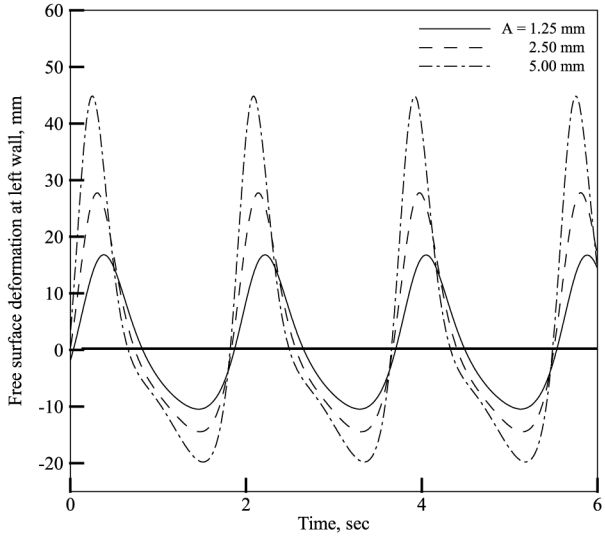

Figure 13.
Effect of amplitude on the steady-state free surface deformation at the left wall ($x = -L/2$), f_e=0.545 Hz, $\Delta t = 0.01$ s, $\Delta\xi = \Delta\eta = 1/20$

References

Abramson, H. (Ed.) (1966), "The dynamic behaviour of liquids in moving containers", NASA SP-106, Washington, DC.

Celebi, M.S. and Akyildiz, H. (2002), "Nonlinear modeling of liquid sloshing in a moving rectangular tank", *Ocean Engineering*, Vol. 29, pp. 1527-53.

Chen, W., Haroun, M.A. and Liu, F. (1996), "Large amplitude liquid sloshing in seismically excited tanks", *Earthquake Engineering and Structural Dynamics*, Vol. 25, pp. 653-69.

Chester, W. (1968), "Resonant oscillations of water waves. II. Experiment", *Proceedings of the Royal Society of London*, Vol. A. 306, pp. 23-39.

Clough, R.W., Niwa, A. and Clough, D.P. (1978), "Experimental seismic study of cylindrical tanks", *J. Struc. Div. ASCE*, Vol. 105, pp. 2565-90.

Cooper, R.M. (1960), "Dynamics of liquids in moving containers", *Journal of American Rocket Society*, Vol. 30, pp. 725-9.

Dutta, S. and Laha, M.K. (2000), "Analysis of the small amplitude sloshing of a liquid in a rigid container of arbitrary shape using a low-order boundary element method", *International Journal for Numerical Methods in Engineering*, Vol. 47, pp. 1633-48.

Floryan, J.M. and Rasmussen, H. (1989), "Numerical methods for viscous flows with moving boundaries", *Applied Mechanics Review*, Vol. 42, p. 323.

Fujino, Y., Sun, L.M., Pacheco, B.M. and Chaiseri, P. (1992), "Tuned liquid damper for suppressing horizontal motion of structures", *ASCE Journal of Engineering Mechanics*, Vol. 118, pp. 2017-30.

Fujii, K., Tamura, Y., Sato, T. and Wakahara, T. (1990), "Wind-induced vibration of tower and practical applications of tuned liquid damper", *Journal of Wind Engineering and Industrial Aerodynamics*, Vol. 33, pp. 263-72.

Hamed, M.S. and Floryan, J.M. (1998), "Numerical simulation of unsteady nonisothermal capillary interfaces", *Journal of Computational Physics*, Vol. 145, pp. 110-40.

Kareem, A. and Sun, W.J. (1987), "Stochastic response of structures with fluid-containing appendages", *Journal of Sound and Vibrations*, Vol. 21, pp. 389-408.

Koh, C.G., Mahatma, S. and Wang, C.M. (1994), "Theoretical and experimental studies on rectangular liquid dampers under arbitrary excitations", *Earthquake Engineering and Structural Dynamics*, Vol. 23, pp. 17-31.

Lamb, H. (1932), *Hydrodynamics*, The University Press, Cambridge.

Lee, S.C. and Reddy, D.V. (1982), "Frequency tuning of offshore platforms by liquid sloshing", *Applied Ocean Research*, Vol. 4, pp. 226-31.

Lepelletier, T.G. and Raichlen, F. (1988), "Nonlinear oscillations in rectangular tanks", *Journal of Engineering Mechanics*, Vol. 114, pp. 1-23.

Matsuuara, Y., Matsumoto, K., Mizuuki, M., Arima, K., Jouuchi, H. and Hayashi, S. (1986), "On a mean to reduce excited vibration with the sloshing in a tank", *J. Soc. Naval. Architecture Japan*, Vol. 160, pp. 424-32.

Miles, J.W. (1976), "Nonlinear surface waves in closed basins", *Journal of Fluid Mechanics*, Vol. 75, pp. 419-48.

Nakayama, T. (1983), "Boundary element analysis of nonlinear water wave problems", *International Journal for Numerical Methods in Engineering*, Vol. 19, p. 953.

Nakayama, T. and Washizu, K. (1981), "The boundary element method applied to the analysis of two-dimensional nonlinear sloshing problems", *International Journal for Numerical Methods in Engineering*, Vol. 17, pp. 1631-46.

Noji, T., Yoshida, H., Tatsumi, E., Kosaka, H. and Hagiuda, H. (1988), "Study on vibration control damper utilizing sloshing of water", *Journal of Wind Engineering*, No. 37, pp. 557-66.

Ohyama, T. and Fujii, K. (1989), "A boundary element method analysis for two-dimensional nonlinear sloshing problem", *JSCE Journal of Structural Engineering*, Vol. 35A, pp. 575-84.

Ramaswamy, B., Kawahara, M. and Nakayama, T. (1986), "Lagrangian finite element method for the analysis of two-dimensional sloshing problems", *International Journal for Numerical Methods in Fluids*, Vol. 6, pp. 659-70.

Reed, D., Yu, J. and Yeh, H. (1998), "Investigation of tuned liquid dampers under large amplitude excitation", *Journal of Engineering Mechanics*, Vol. 124, pp. 405-13.

Shimizu, T. and Hayama, S. (1987), "Nonlinear responses of sloshing based on the shallow water theory", *JSME International Journal*, Vol. 30, pp. 806-13.

Soong, T.T. and Dargush, G.F. (1997), *Passive Energy Dissipation Systems in Structural Engineering*, Wiley, Chichester.

Sun, L.M. and Fujino, Y. (1994), "A semi-analytical model for tuned liquid damper (TLD) with wave breaking", *Journal of Fluids and Structures*, Vol. 8, pp. 471-88.

Sun, L.M., Fujino, Y. and Koga, K. (1995), "A model of tuned liquid damper for suppressing pitching motions of structure", *Earthquake Engineering and Structural Dynamics*, Vol. 24, pp. 625-36.

Sun, L.M., Fujino, Y., Pacheco, B.M. and Isabe, M. (1989), "Nonlinear waves and dynamic pressures in rectangular TLD-simulation and experimental verification", *Journal of Structural Engineering and Earthquake Engineering*, Vol. 6, pp. 251-62, *Proc. JSME*.

Tait, M.J., El Damatty, A.A. and Isyumov, N. (2001), "The effectiveness of a tuned liquid damper", *Proceedings of the 29th Annual Canadian Society for Civil Engineering Conference*, A63, Victoria, British Columbia.

Tamura, Y., Fujii, K., Sato, T., Wakahara, T. and Kosugi, M. (1988), "Wind-induced vibration of tall towers and practical applications of tuned sloshing damper", *Proceedings of the Workshop on Serviceability of Buildings*, Ottawa, Ontario, pp. 228-41.

Tosaka, N. and Sugino, R. (1991), "Boundary element analysis of potential flow with nonlinear free surface", *Proceedings of the 4th China-Japan Symposium on Boundary Element Methods*, pp. 137-44.

Vandiver, J.K. and Mitone, S. (1978), "Effect of liquid storage tanks on the dynamic response of offshore platforms", *Applied Ocean Research*, Vol. 1, pp. 67-74.

Watanabe, S. (1969), "Methods of vibration reduction", *Proc. Japan Naval Arch. Soc. Symp.*, pp. 156-89.

Wakahara, T. (1993), "Wind-induced response of TLD-structure coupled system considering non-linearity of liquid motion", *Shimizu Tech. Res. Bull.*, Vol. 12, pp. 41-52.

Wakahara, T., Ohyama, T. and Fujii, K. (1992), "Suppression of wind-induced vibration of a tall building using tuned liquid damper", *Journal of Wind Engineering and Industrial Aerodynamics*, Vol. 41-44, pp. 1895-906.

Warnitchai, P. and Pinkaew, T. (1998), "Modeling of liquid sloshing in rectangular tanks with flow-dampening devices", *Engineering Structures*, Vol. 20, pp. 593-600.

Zang, Y., Xue, S. and Kurita, S. (2000), "A boundary element method and spectral analysis model for small-amplitude viscous fluid sloshing in couple with structural vibrations", *International Journal for Numerical Methods in Fluids*, Vol. 32, pp. 79-96.